metals

MDPI

Article

Analysis on the Quenching Deformation Characteristics of Light Cast Aluminum Alloy Wheels and Their Control Strategies

Hui Chi [1,2], Meng Yan [1,3,*], Zhengqi Xu [1,4], Pengfei Xiang [1,4], Zijun An [1] and Huagui Huang [1,4]

1 School of Mechanical Engineering, Yanshan University, Qinhuangdao 066004, China
2 CITIC Dicastal Co., Ltd., No 185, Long Hai Road, Economic and Technological Development Zone, Qinhuangdao 066011, China
3 Hebei Innovation Center for Equipment Lightweight Design and Manufacturing, Yanshan University, Qinhuangdao 066004, China
4 National Engineering Research Center for Equipment and Technology of Cold Rolled Strip, Yanshan University, Qinhuangdao 066004, China
* Correspondence: yanm@ysu.edu.cn

Abstract: The purpose of this paper is to develop a new technology for controlling the quenching deformation of light cast aluminum alloy wheels. First, based on the existing wheel heat treatment process, a gas–liquid–solid multi-phase flow coupling model was established through the ANSYS Workbench platform to analyze the gas–liquid phase change, heat exchange on wheel surface and quenching deformation characteristics during the process of wheel immersion into the water. The results show that heat exchange characteristics of the wheel surface are comprehensively affected by wheel structure, quenching fluid flow field and gas–liquid phase transition. There are a lot of non-uniform heat exchange areas in the outer rim, spoke area and center area, which affect the overall deformation characteristics. Affected by spoke structure, the maximum deformation occurs at the outer and inner rim end faces farthest away from the wheel. Based on the above research, this paper independently develops a new deformation control strategy of spray and water immersion composite step process. Through spraying, the influence of spoke structural stiffness on the overall deformation characteristics of the wheel is effectively reduced, and the wheel deformation control is realized by meeting the mechanical properties of the wheel, with the maximum deformation reduction of 39.2%. This study provides a new option for the integrated control of deformation and mechanical properties of aluminum alloy wheels.

Keywords: aluminum alloy wheel; deformation control; quenching simulation; heat treatment

check for updates

Citation: Chi, H.; Yan, M.; Xu, Z.; Xiang, P.; An, Z.; Huang, H. Analysis on the Quenching Deformation Characteristics of Light Cast Aluminum Alloy Wheels and Their Control Strategies. *Metals* **2023**, *13*, 128. https://doi.org/10.3390/met13010128

Academic Editor: Babak Shalchi Amirkhiz

Received: 23 November 2022
Revised: 26 December 2022
Accepted: 5 January 2023
Published: 8 January 2023

Copyright: © 2023 by the authors. Licensee MDPI, Basel, Switzerland. This article is an open access article distributed under the terms and conditions of the Creative Commons Attribution (CC BY) license (https://creativecommons.org/licenses/by/4.0/).

1. Introduction

Aluminum alloy wheels have many advantages, such as low cost, light weight, high strength, good heat dissipation and recyclability, and have been widely accepted by the domestic and international automotive industries. They are of great significance for lightweight vehicles, fuel consumption reduction, energy saving, emission reduction and driving experience improvement [1–4]. Their production process includes melting, casting, heat treatment, machining, painting, finished product packaging and other processes. At this stage, the T6 heat treatment process is mainly used to control mechanical properties, resulting in a wheel with excellent overall performance [5,6]. However, the negative effect of T6 heat treatment is deformation, which accounts for 40–50% of the whole deformation in the whole production process. With the rapid development of new-energy vehicles and the promulgation of stringent carbon emission regulations, the reduction of structural stiffness caused by the reduction of wheels has further aggravated heat treatment deformation and led to the reduction of yield, which has become a major problem in the manufacturing process of aluminum alloy wheels. Therefore, it is an urgent scientific problem for aluminum

alloy wheel manufacturers to study the deformation characteristics of the wheel quenching process, to guide the deformation control and at the same time improve the material saving rate and product yield [7].

The quenching process is a dynamic process involving the coupling of the temperature field and stress field. The quenching process includes fluid flow, boiling heat transfer, and fluid and convection heat transfer between fluid and solid. The heat transfer mechanism is very complex [8]. The surface heat transfer coefficient is an important boundary condition of the temperature field. The cooling curve is obtained by an end quenching test according to the cooling form, and then the heat transfer coefficient under one-dimensional heat transfer is calculated by inverse heat conduction. It is used as the third boundary condition to carry out thermo-mechanical coupling modeling and simulation to study the hardenability and residual stress distribution of materials, and to achieve a controlled shape control of plates and profiles [9]. The rapid development of computational fluid dynamics has become an important research method [10–14]. Song, J.S and others have taken boiling heat transfer and two-phase flow into consideration. The dynamic process of entering water and quenching of forged aluminum alloy wheels has been simulated by means of three-dimensional dynamic grid technology and fluent software. They focus on the temperature change of wheels during the quenching process and the change of the flow and temperature field of fluids in the quenching tank to guide the design of the quenching tank structure [15]. Compared with forged aluminum alloy wheels, cast aluminum alloy wheels have a more complex topological structure, which makes a large difference in the cooling process between wheels with different characteristic structures. At present, there is little research on the temperature and stress variety, wheel deformation characteristics, deformation mechanism and control mechanism in the dynamic process of casting aluminum alloy wheel quenching.

In this paper, a gas–liquid–solid multi-phase flow coupling model is established based on the Workbench platform to analyze the gas–liquid phase change, heat exchange on wheel surface and quenching deformation characteristics during the wheel entering water inflow process. Based on this, a heat treatment test platform was independently developed to carry out the research on the composite step quenching process of immersion in water and spray and immersing water, aiming at providing a new alternative for the integrated control of the shape and mechanical properties of aluminum alloy wheels.

2. Mathematical Model of Multi-Phase Coupled Heat Exchange

The quenching process of high temperature wheels immersed into water involves flow and heat transfer problems. Water vapor is generated on the wheel surface to form bubbles, which grow up, rise and break gradually to take away heat. Meanwhile, convection heat exchange exists between the water and wheel. In the whole process, the multiphase flow field is considered as a turbulent flow field with a fixed three-dimensional viscosity constant. Fluids are simplified as incompressible fluids, and the turbulence model uses Realizable k-ε, a two-equation model in which the transport equation is [16].

$$\mathrm{div}(\rho \boldsymbol{u} \boldsymbol{\Psi}) = \mathrm{div}(\Gamma grad \boldsymbol{\Psi}) + \boldsymbol{S} \tag{1}$$

ρ is the fluid density; $\boldsymbol{u} = (u, v, w)$ is the velocity vector of flow field, m/s; $\boldsymbol{\Psi}$ is Flux of flow field; $\boldsymbol{S}$ is the source term of the mass conservation equation; Γ is the diffusion coefficients of the k-ε equations, m^2/s.

During quenching, phase transition does not occur in the aluminum alloy, and the whole system is transient without internal heat source. The differential equation of heat conduction based on Fourier's law is [17].

$$\mathrm{div}(\lambda \mathrm{grad} T) = \rho C_P \partial T / \partial t \tag{2}$$

In the equation, λ is the thermal conductivity, W/(m·°C); ρ is the density, kg/m^3; C_P is the specific heat capacity, J/(kg·°C); T is the transient temperature of the object,·°C; t is time for the heat transfer process, s.

During immersion quenching, the energy exchange and transfer of flow, solid and heat fields occur simultaneously on the wheel surface, which is complex. The energy conservation law [18] is observed on the fluid–solid heat transfer boundary and is calculated by Equation (3).

$$q/_{solid}^{wall} = q/_{fluid}^{wall} \tag{3}$$

A thin layer, called a boundary layer, forms on the wheel surface. The boundary layer is considered to be immobile with respect to the wall. In order for a solid to transmit heat to a fluid on the boundary layer, the heat must pass through the boundary layer and heat transfer occurs between the solid surface and the boundary layer. This is obtained by Fourier's law.

$$q/_{solid}^{wall} = -\lambda \nabla T \tag{4}$$

In the equation, λ is the thermal conductivity, W/(m·°C); normal temperature gradient of the boundary layer.

Forced convection heat transfer occurs at the interface between the flow fluid and the boundary layer, which is derived from Newton's cooling law:

$$q/_{\text{fluid}}^{wall} = h(T_\text{s} - T_\text{ref}) \tag{5}$$

In the equation, T_s is the surface temperature of the boundary layer, °C; T_ref is the temperature of the flowing fluid, °C. h is the heat exchange coefficient, W/(m^2·°C).

Cast aluminum alloys are elastic–plastic isotropic materials and their plastic deformation is described by the Extended Ludwik–Hollomon model [19].

3. Establishment and Calculation of Fluid Calculation Domain Model

3.1. Fluid Area Gridding

The cast aluminum alloy wheel structure includes the inner flange, rim, outer flange, window, spoke, mounting area, etc. The complex surface of the blue part shown in Figure 1 is partially trimmed by CATIA software to converge the calculation.

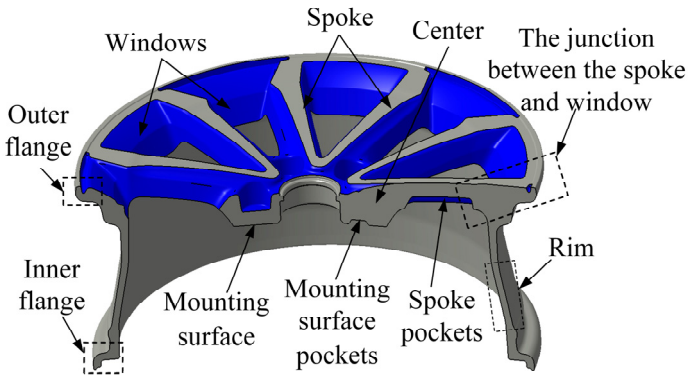


Figure 1. Schematic diagram of aluminum alloy wheel structure.

In the actual quenching process, shown in Figure 2a, the wheels are gradually immersed in water from above. To simplify the calculation of the wheel motion, water is gradually immersed over the wheels from below to above. The simulation area is modeled and meshed as a whole with 3–4 layers of boundary layers on the wheel surface. The mesh type is tetrahedron and the total number of elements is 1,428,024. The computational domain grid is shown in Figure 2b.

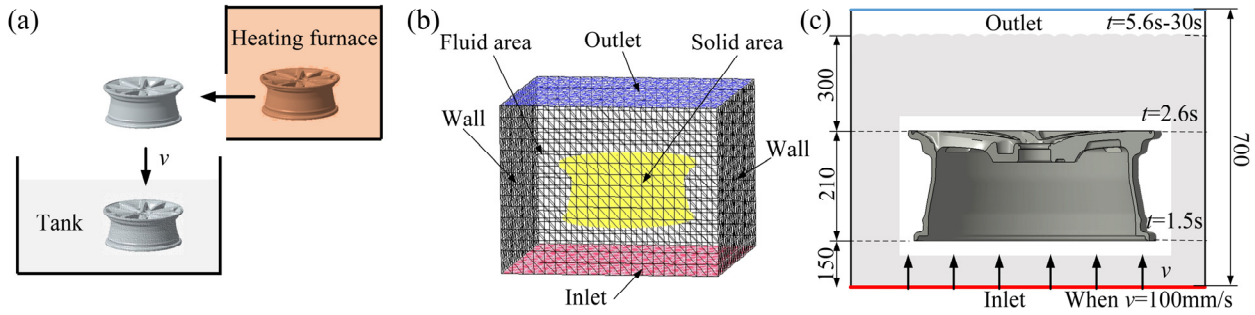


Figure 2. Immersion process and calculation model: (**a**) actual quenching process schematic diagram, (**b**) computational domain grid, (**c**) position of the water surface at each time.

3.2. Setup of Workbench Model

Immersion quenching Finite Element Modeling is transient, open gravity option, gravity acceleration is 9.81 m/s^2, the multiphase flow, energy and turbulence equations are open. There are two phases of liquid water and water vapor in the multiphase flow equation, in which the transformation equation of liquid water and water vapor is the evaporation/condensation model. The turbulence equation is Realizable k-ε and Standard model, and the solution method is set as SIMPLE algorithm.

3.3. Fluid Properties and Boundary Conditions

The quenching process of aluminum alloy wheels is a dynamic process, which involves convection heat exchange of water and phase transition of water to steam. The density of water and steam is set as a constant of 971.7 kg/m^3 and 0.5542 kg/m^3. Other thermos-physical parameters are set as a variable with temperature [20].

The quenching water tank is initially set as water vapor with a temperature of 40 °C. The water temperature is 80 °C, the inlet flow rate is 100 mm/s, the flow rate is 0 mm/s after the water has passed the wheel 300 mm, and the total duration is 30 s. The corresponding position of the water surface at each time is shown in Figure 2c.

3.4. Solid Properties and Boundary Conditions

The solid state is A356 cast aluminum alloy. Based on the measured chemical composition as Table 1, JMatPro simulation software is used to calculate the temperature-related attribute parameters [21]. Multiple function fitting is carried out between 25 °C and 545 °C and the independent variable is the temperature function as Table 2. The initial temperature is set at 540 °C.

Table 1. Chemical composition of A356 casting aluminum alloy (wt. %).

Chemical Element	Al	Si	Fe	Cu	Mn	Mg	Zn	Ti	Sr
Standard	≥90	6.5~7.5	≤0.20	≤0.10	≤0.10	0.25~0.45	≤0.10	0.08~0.20	0.008~0.20
Measured	92.7	6.73	0.11	0.004	0.002	0.278	0.005	0.115	0.001

Table 2. Temperature-dependent formula properties of A356 casting aluminum alloy.

Parameter	Functional Relationship	R-Square
Specific heat capacity (J/(kg·°C))	$873.7 + 0.6764\,T - 9.9866 \times 10^{-4}\,T^2 + 1.1926 \times 10^{-6}\,T^3$	0.99991
Density (kg/m^3)	$2685.6 - 0.1683\,T - 6.3294 \times 10^{-5}\,T^2$	1
Thermal conductivity (W/(m·°C))	$183.25 + 4.50 \times 10^{-2}\,T - 2.1161 \times 10^{-4}\,T^2 + 1.5977 \times 1\,0^{-7}\,T^3$	0.99931
Poisson's ratio	$0.3305 + 3.3373 \times 10^{-5}\,T + 3.7497 \times 10^{-8}\,T^2$	1
Young's modulus (MPa)	$71{,}642.9 - 31.7224\,T - 2.19 \times 10^{-2}\,T^2$	1

4. Analysis of Simulation Results

4.1. Analysis of Heat Transfer Characteristics of Inflow Flow

The temperature, vapor volume fraction and fluid velocity of all parts in the three-dimensional area of the whole model can be obtained by numerical simulation calculation. From the water vapor volume fraction cloud shown in Figure 3, it can be seen that water vapor is generated quickly when it contacts the wheel surface and increases with the contact area. When the wheel is completely immersed in the water, more water vapor is generated in the large area where the wheel center and spokes combine with the window. As the immersion time increases, the water vapor gradually decreases. As can be seen from Figure 4, bubbles are generated when water contacts the wheel surface and the steam flow rate increases with it. At 6 s to 8 s, the steam flow rate reaches its maximum value.

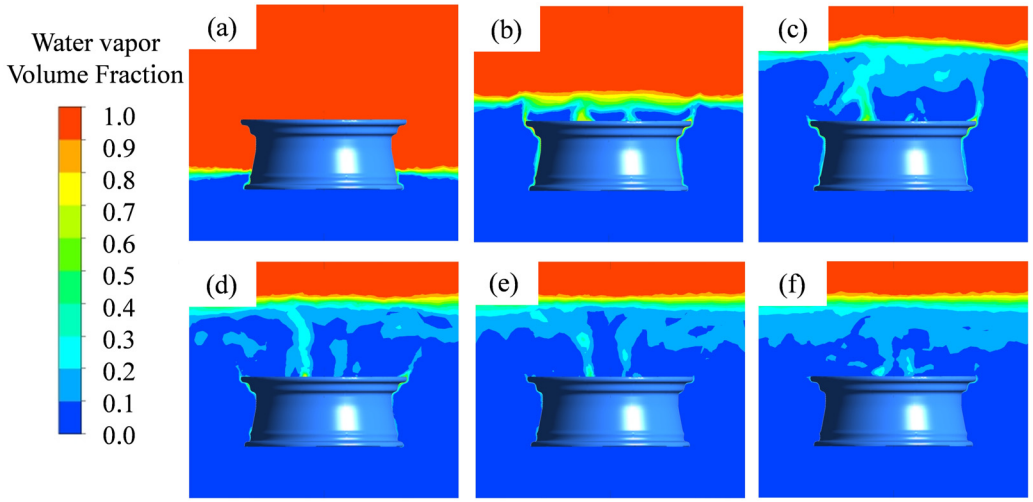


Figure 3. Water vapor volume fraction at different times: (**a**) 2 s, (**b**) 4 s, (**c**) 6 s, (**d**) 8 s, (**e**) 10 s, (**f**) 12 s.

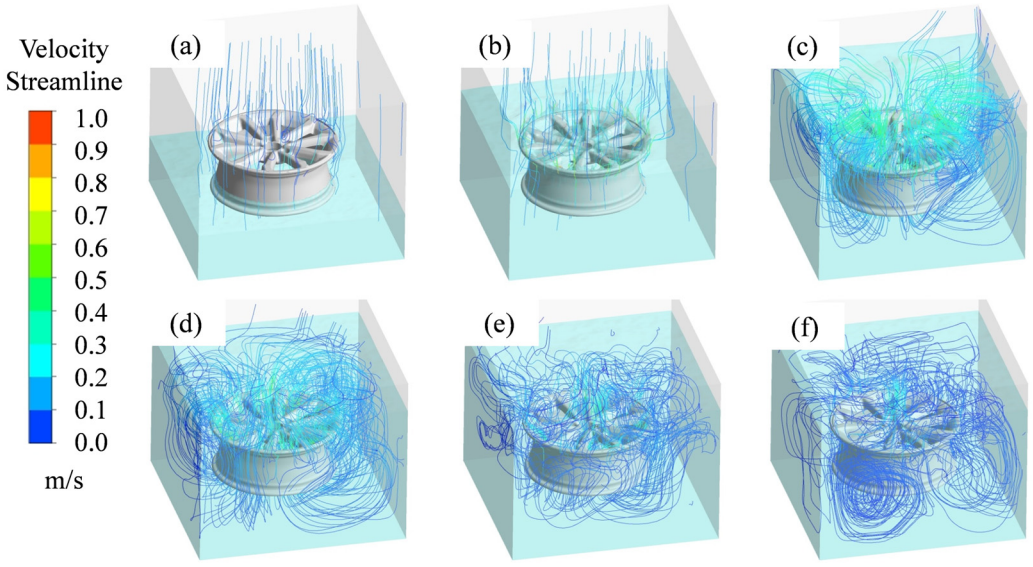


Figure 4. Flow diagram of fluid velocity at different times: (**a**) 2 s, (**b**) 4 s, (**c**) 6 s, (**d**) 8 s, (**e**) 10 s, (**f**) 12 s.

4.2. Analysis of Heat Exchange Characteristics on Wheel Surface

During the wheel immersion quenching process, the fluid contacts the wheel directly, and heat conduction and convection occur simultaneously. The calculated heat transfer coefficient of the wheel surface is shown in Figure 5. The heat transfer difference between different areas of the wheel is obvious at different times. The surface and heat transfer char-

acteristics of each characteristic structure show great differences, of which the maximum heat transfer coefficient is 6500 W/(m^2·°C).

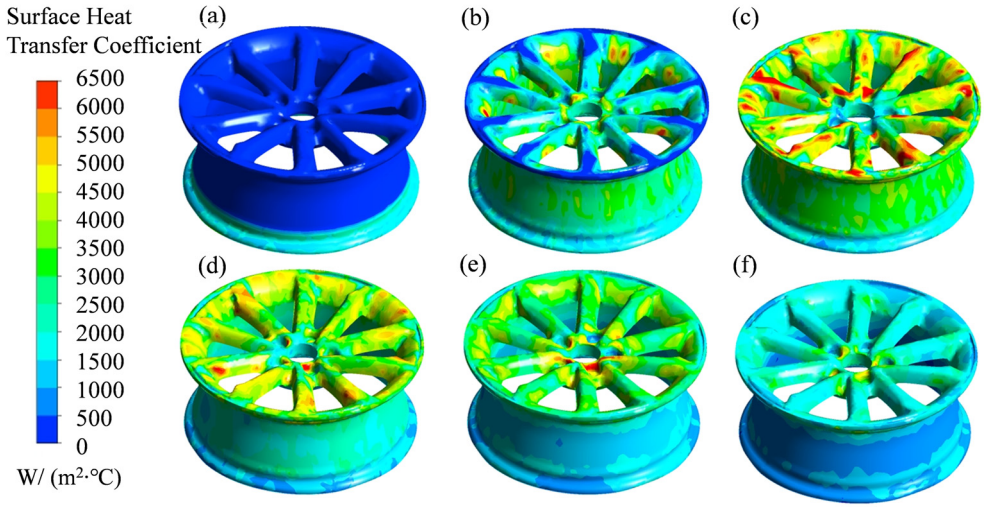


Figure 5. Cloud image of surface of heat transfer coefficient at different times: (**a**) 2.5 s, (**b**) 4 s, (**c**) 6 s, (**d**) 8 s, (**e**) 10 s, (**f**) 12 s.

4.3. Analysis of Quenching Deformation Mechanism

The temperature difference of each structure during the quenching process are quite large, and temperature curves are shown in Figure 6. Point E possess the maximum thickness at the junction of spoke and window, and the other seven points are 5 mm away from the outer surface. After 1.5 s from beginning, the inner rim first comes into contact with water and the temperature begins to drop. At 6.5 s, the whole wheel presents a large temperature gradient. The wall thickness of point G on rim is thinner and the temperature drop is the fastest. Affected by the weight reduction socket of the spoke, the wall thickness of point C in the middle of the spoke is thinner and its temperature drop is faster than that of points E and B on both sides. The hub is relatively thick and the surface area in contact with water is small, so point A's cooling is slowest.

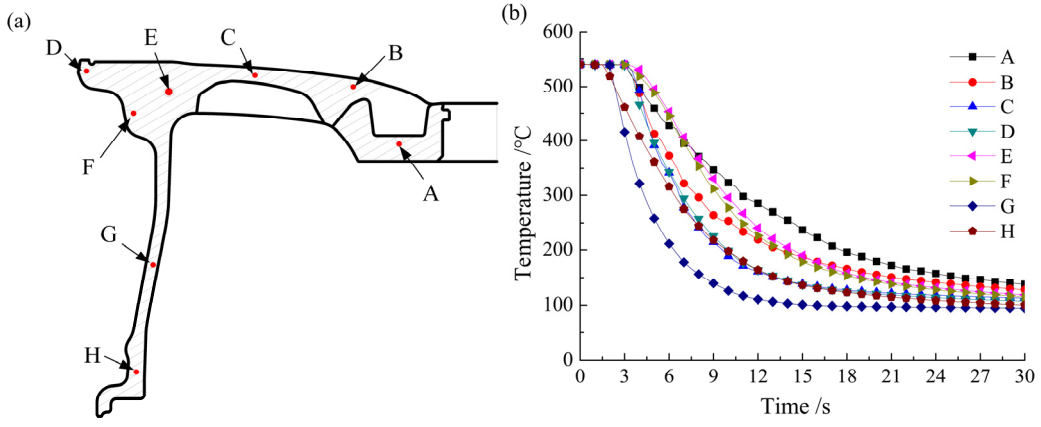


Figure 6. Cooling curve of characteristic positions: (**a**) Position of key points, (**b**) Simulation temperature.

The temperature field and heat transfer coefficient of the wheel mesh are taken as the third boundary condition to carry out thermal stress analysis. It can be seen that the deformation occurs on the end face of the outer wheel rim and this is the maximum deformation position. In Figure 7, the stress values and temperature values of the outer and inner rim end surfaces are extracted clockwise and counterclockwise from the valve position, respectively. As a result, in Figure 8, the stress values of the rim edges corresponding to the spoke positions are higher than those of the adjacent windows. Based on the analysis of

wheel structure, it can be seen that during quenching, the deformation of the outer rim is affected by the structural stiffness of the whole structure composed of the hub, spoke and the combination of spoke and window section, and the inner rim shows the deformation characteristics similar to that of the outer rim.

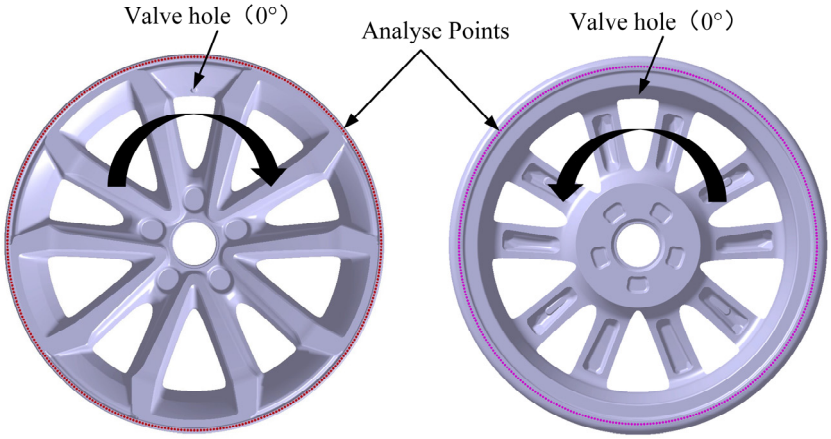


Figure 7. Analyses points of outer flange and inner flange.

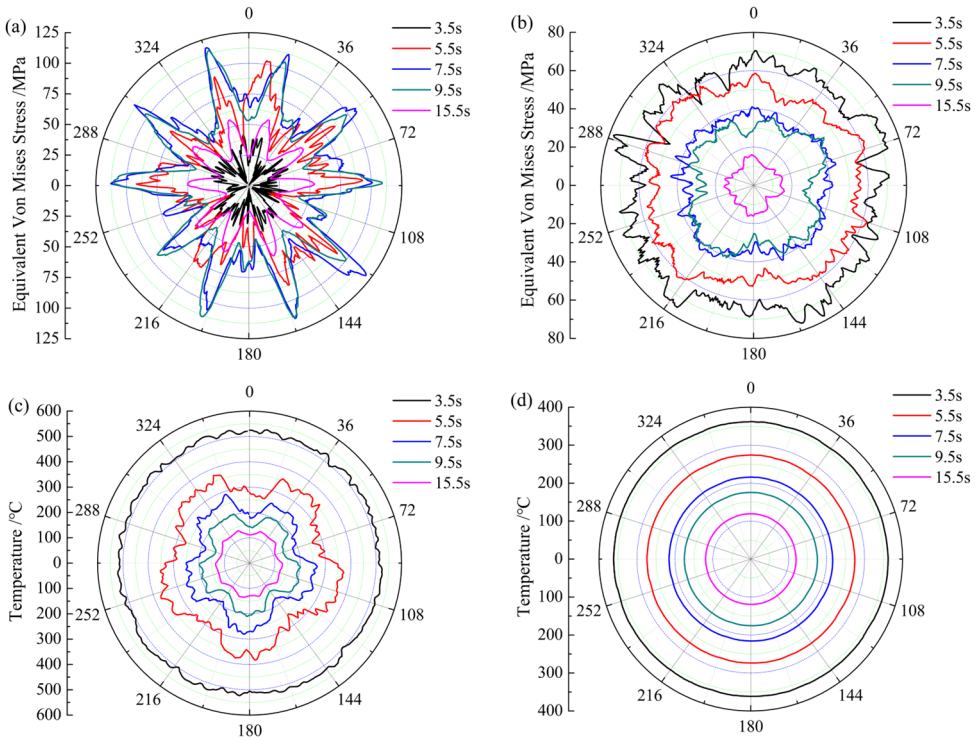


Figure 8. Analyses results of outer and inner flange: (**a**) Equivalent Von Mises Stress on outer flange, (**b**) Equivalent Von Mises Stress on inner flange, (**c**) Temperature on outer flange, (**d**) Temperature on inner flange.

During the whole quenching process, when water acts as a quenching medium and heat exchanges with the wheel, there are some influencing factors, such as physical properties of the fluid, shape of the heat exchange surface, flow rate difference of fluid in different parts, etc. The complexity of the wheel structure makes each part of the wheel have an uncoordinated shrinkage process, especially the large force and reaction force between the spoke and window section. The force among the 10 spokes is not equal due to the difference of structure and size in the actual casting products, which finally leads to large unstable deformation, which is mainly reflected in the outer and inner rims of the outermost end of near-acting force. The deformation mechanism is shown in Figure 9. Therefore, a better

deformation controlling strategy is to have a lower cooling process on the front surface before immersing into the water, such as the spray and water quenching process.

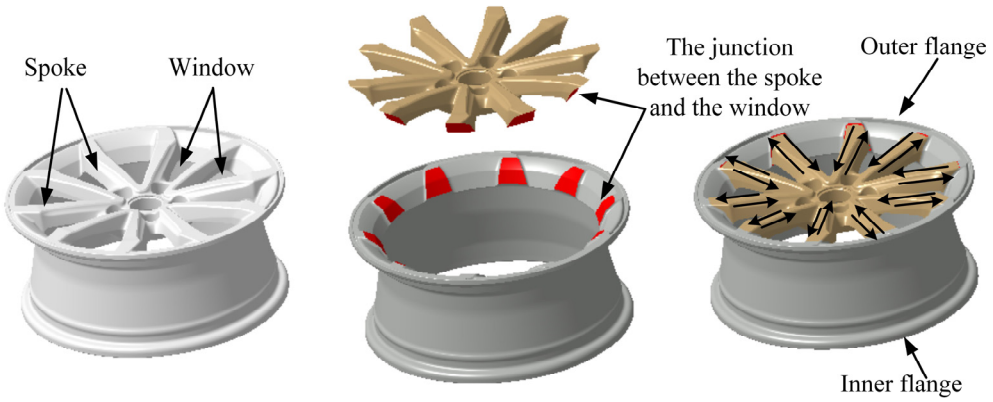


Figure 9. Schematic diagram of wheel submerged quenching deformation.

5. Tests and Measurements

5.1. Introduction to Test Wheel and Heat Treatment Platform

In order to accurately analyze the quenching deformation characteristics and temperature changes of the wheels, the deformation of the cast revolving surface is removed by a turning process and the 17-inch wheels required for the test are obtained. A test platform for quenching heat treatment of aluminum alloy was established. As shown in Figure 10a, the main body of the platform is composed of the fast feeding and water conveying mechanism, heating furnace, constant temperature water tank, spray cooling structure (with opening in Figure 10b), data acquisition system, etc. Among them, the PLC control system is used by the rapid feeding and water inflow conveying mechanism to ensure the process stability.

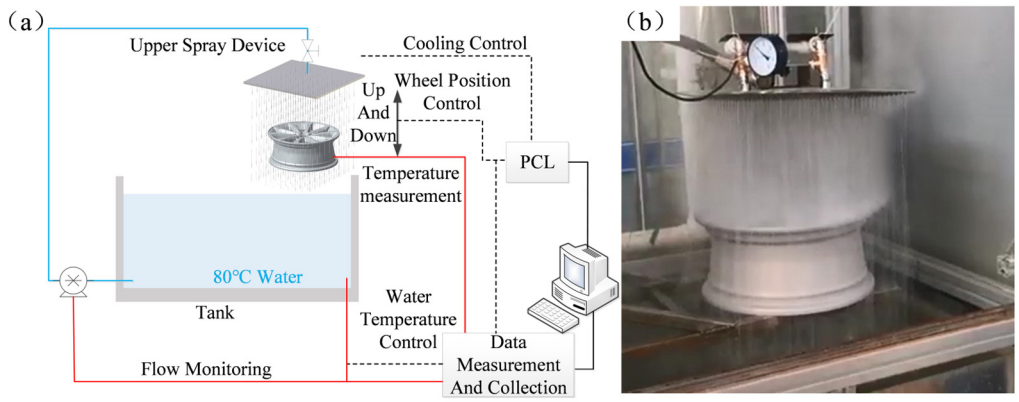


Figure 10. Heat treatment test device: (**a**) Schematic diagram, (**b**) Spraying process before water immersion.

In order to accurately monitor the change in the wheel quenching temperature, a K-type thermocouple with a diameter of 0.5 mm is selected as a temperature sensor to measure the temperature of monitoring points A, B, C, E, F, G and H during the quenching process. Repeat the measurement three times to obtain the average value. The results of measured and simulated temperatures at each monitoring point are compared and the maximum temperature difference is within −8.7%. Therefore, the analysis of the coupled heat transfer by heat flow is accurate and reliable.

5.2. Wheel Deformation Measurement

First, the three-dimensional point cloud model of the wheel obtained by the handheld three-dimensional laser scanner (Handyscan3D) is imported into the Ploy works software,

and then the flange surface is taken as the datum. By comparing the tested wheel with the theoretical model, the scanning results are obtained, as shown in Figure 11. The maximum position of wheel deformation occurs in the inner/outer rim area as the machining datum, which is consistent with the position of simulation results.

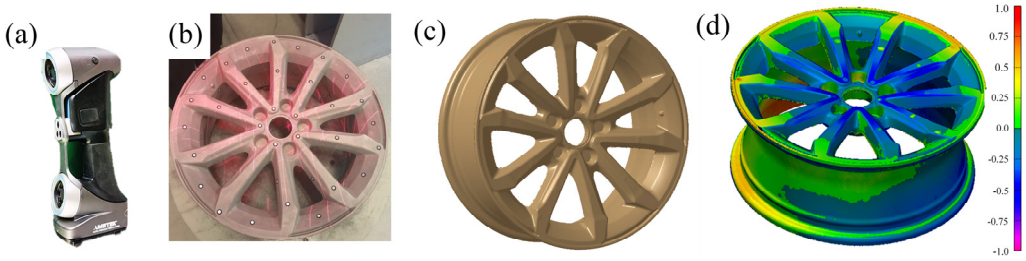


Figure 11. The 3D scan process and result: (**a**) Handyscan3D, (**b**) Scanning the wheel, (**c**) Scanning result, (**d**) Final scanning result after comparison.

In order to accurately analyze the heat treatment deformation characteristics of aluminum alloy wheels and avoid the problem of the insufficient precision of the 3–6 mm wide rim area by 3-D laser scanner, the outer, inner and rim edges of the tested wheels were measured with a Coordinate Measuring Machine (CMM) inspection contact measuring machine, and the results are shown in Figure 12. Combined with the result of 3D scanning, it is indicated that the wheel becomes ellipsoid during quenching, and the deformation degree is more severe and the deformation mechanism is more complex.

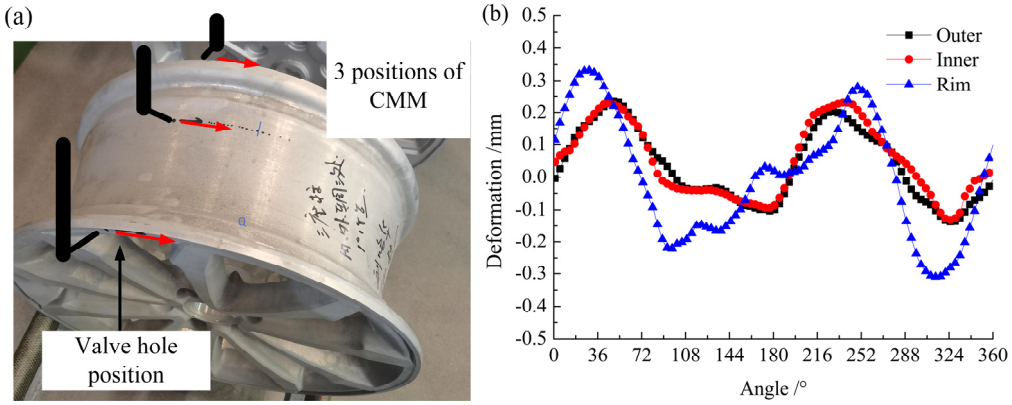


Figure 12. CMM measuring: (**a**) Measuring positions, (**b**) Measuring results.

5.3. Control Strategy for Wheel Deformation

A new type of composite step hardening process with spray and water is adopted, i.e., spraying for 15 s before immersion, cooling the outer rim, spoke and center at a lower cooling rate to reduce the deformation from the whole quenching process.

Referring to the existing heat treatment process, the aluminum alloy wheels are heated to 540 °C in the heating furnace for 280 min. Then, the wheels are moved over the quenching water tank for direct water quenching and graded and partitioned cooling spraying with 15 s + water. Then, the aging treatment is carried out. Then, the outer wheel rim end surface of the wheels is measured with the coordinate measuring machine. The test conditions are shown in Table 3. The results show that the combined step hardening process improves the end deformation by 39.2%, of which six test wheels have the end deformation of the outer wheel flange, as shown in Figure 13.

Table 3. Deformation of outer end face comparison of different heat treatment processes.

Technics Number	Quenching Processes	Transfer Time/s	Average Deformation/μm	Relative Improvement/%	Numbers of Wheel	Wheel Number
1	Water	25	470	Baseline	3	1#, 2#, 3#
2	Spraying 15 s + water	40	275	39.2	3	4#, 5#, 6#

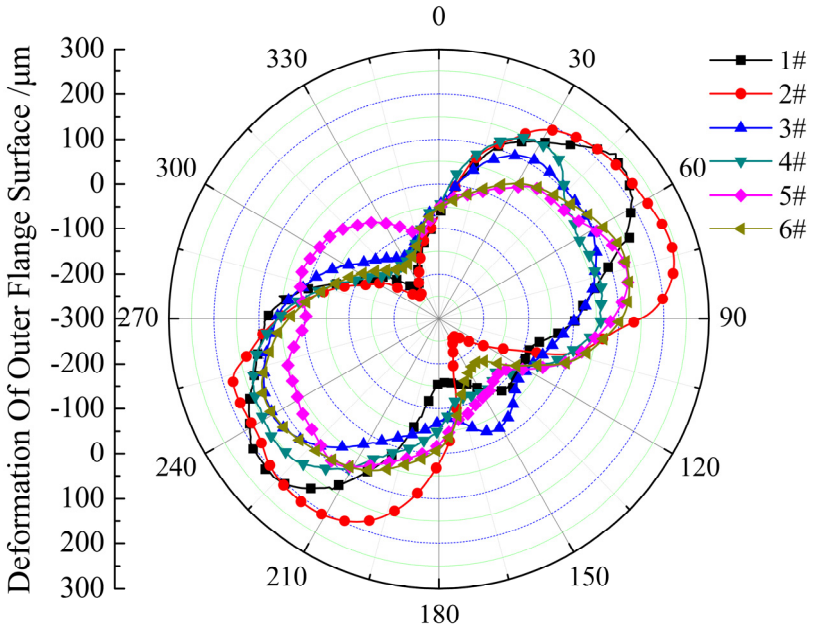


Figure 13. Deformation on outer end face under different quenching processes.

5.4. Analysis of Structure and Mechanical Properties of Wheels

The deformed wheels are transferred to the coating process of the aluminum alloy wheel production line to obtain the wheels with specific finished product properties, so as to ensure that the structure and mechanical properties of the wheels meet the technical requirements of the automobile factory. Five typical locations, such as center, spoke, inner flange, outer flange and rim, are selected to test the tensile mechanical properties, hardness and micro characteristics according to ISO 6892-1 and ISO 6506-1 standards. Cylindrical compression test specimens of 80 mm length and 5 ± 0.02 mm diameter were machined from five typical locations of two wheels. Two stretch bars are taken from one typical location of each wheel. Limited by the rim wall thickness, no tensile specimens were taken at the rim. A Zwick universal testing machine with 0.17 mm/s was used to obtain the yield strength, elongation and tensile strength in Figure 14. The Brinell hardness was measured by a Wilson Wolpert Brinell hardness tester on a 10 × 10 × 10 mm part with HB 5/250 method, four points are taken from one part, the first point is excluded and the remaining three points are averaged. The microstructures of the samples have been characterized using an Axiover-200MAT metallographic microscope. The samples were cut by wire electric discharge machine to 10 × 10 × 10 mm, then prepared by grinding disks, and polished and finally etched with absolute ethanol and dried with a dryer, 0.5% HF acid solution [22].

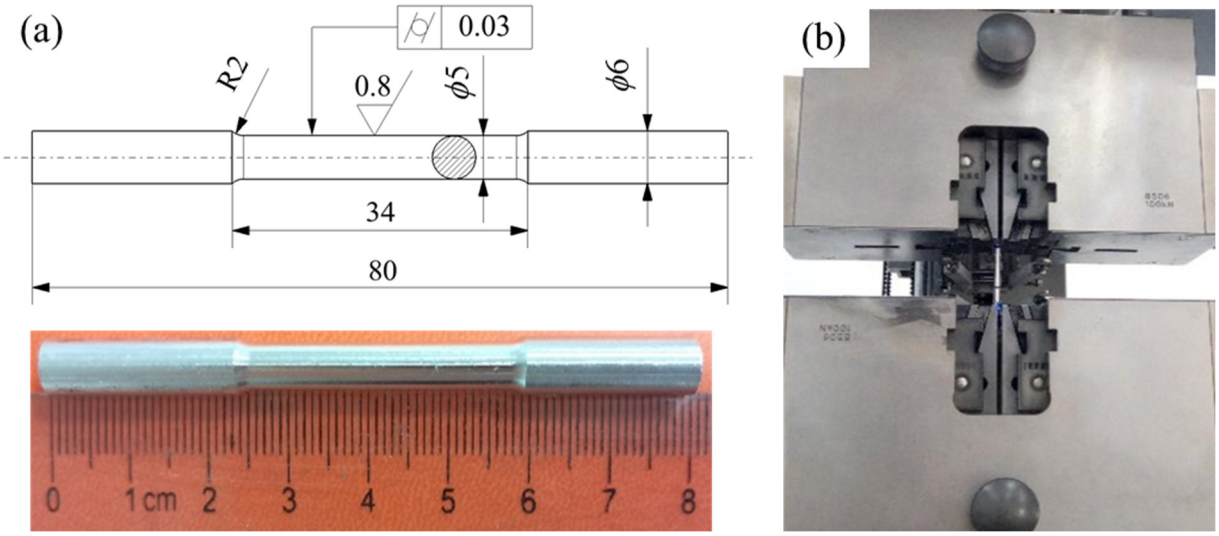


Figure 14. Stretch bars for mechanical properties: (**a**) Stretch sample bar size, (**b**) Tensile testing equipment.

Figure 15 shows the microstructures of five typical locations of aluminum alloy wheels under processes 1 and 2, which are mainly determined by α- Al, eutectic silicon and a small amount of Mg_2Si. Affected by the thickness difference of each part of the wheel, the cooling rates of the rim, spoke and center decrease in turn, the grain size increases in turn, and the number and shape of precipitated phases are different during casting and quenching, which shows different mechanical properties. Comparing with the results of normal water immersion and graded heat treatment, it can be seen that the structure characteristics of the main cooling areas in the spraying stage are slightly different in the center, spoke and outer rim, while the precipitation of Si element in the structure grain boundaries in the non-intervened areas such as inner rim and rim is significantly increased. Under the two heat treatment processes, the performance test results for different parts of the wheel are shown in Figure 16. When spraying is included, the yield strength, tensile strength and hardness decrease as a whole and the elongation increases as compared with the direct water inflow process. With the addition of the spraying process, spokes and outer rims are first cooled by water with low strength, while rims and inner rims are in an air-cooled state, and a small amount of second phase precipitates in advance before water entry, so the strength decreases and elongation increases. It is worth noting that the yield strength of the inner wheel rim area decreases by the largest amount to 6.2%, which is due to the influence of the wheel structure, spray position and wheel posture at this time. During the spraying process, water does not reach the inner wheel rim, even drips or evaporates before reaching the rim, and the transfer time is prolonged by 15 s, which makes the solution more inadequate and results in strength loss.

However, the mechanical properties of aluminum alloy wheels still meet the requirements of automobile factories. In the follow-up, the strength of the inner rim can be improved by improving the continuity of equipment and shortening the transfer time. In conclusion, it is indicated that the improved step heat treatment process can be used as a new direction for the integrated control of heat treatment formality of alloy wheels.

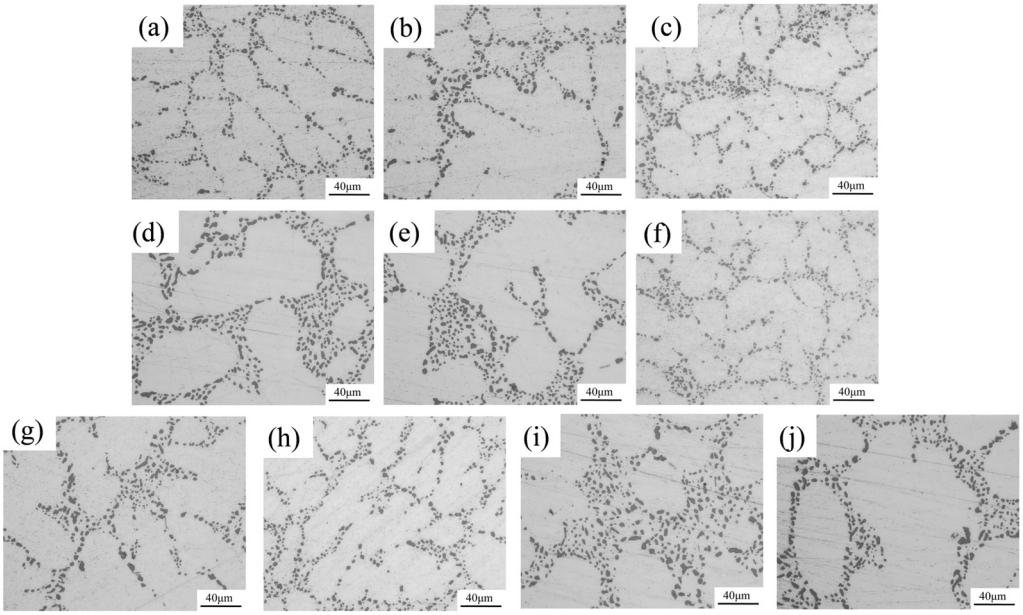


Figure 15. Comparison of microstructure of heat treatment showing α-Al (bright), Al–Si eutectic (dark) phases: (**a**–**e**) water immersion, (**f**–**j**) spray 15 s and water immersion, (**a**,**f**) inner flange, (**b**,**g**) Rim, (**c**,**h**) Outer flange, (**d**,**i**) Spoke, (**e**,**j**) Center.

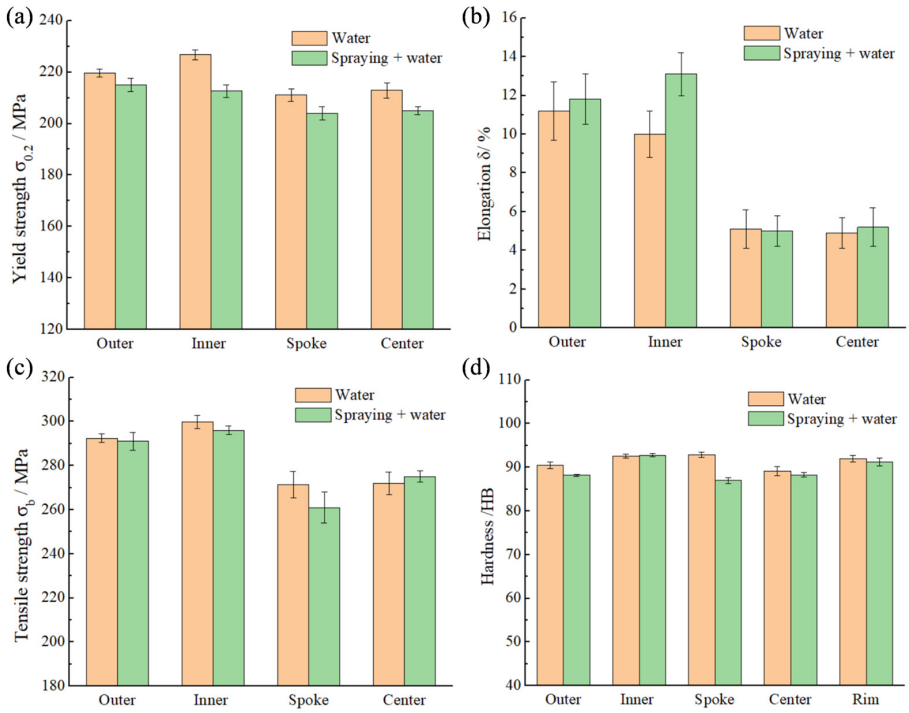


Figure 16. Comparison of mechanical properties: (**a**) Yield strength, (**b**) Elongation, (**c**) Tensile strength, (**d**) Hardness.

6. Conclusions

In this paper, a heat–fluid–solid coupling simulation model of a water immersion quenching process and a new type of composite step hardening process with a spray and water test platform for a light cast aluminum alloy wheel were independently established. Through the simulation analysis of quenching deformation characteristics, experimental exploration of new quenching process and the performance test characterization, the quenching heat transfer mechanism and deformation control strategy of light cast aluminum alloy wheel were accurately constructed. The main conclusions are as follows:

(1) Based on Workbench platform, the immersion quenching process was simulated by multi-physical field coupling, and the change characteristics of physical fields and the heat treatment deformation mechanism during the whole quenching process were revealed.
(2) The deformation characteristics of the inner/outer rim end face are affected by the stiffness of the wheel structure, and the deformation of the inner rim presents the deformation characteristics following with the outer rim. However, affected by the uneven heat exchange of the wheel and internal structure defects, the overall deformation presents the characteristics of double-peak and trough.
(3) The mechanical properties and hardness indexes of each monitoring point of the new graded zone quenching process spraying 15 s and water immersion can meet the automobile factories' requirements for an aluminum alloy wheel. The maximum reduction of the wheel end deformation is 39.2%, which can be used as a new direction of integrated regulation and control of heat treatment formality.

Author Contributions: Conceptualization, H.H. and H.C.; methodology, M.Y. and Z.A.; software, Z.X. and H.C.; validation, M.Y. and P.X.; writing—original draft preparation, H.C.; writing—review and editing, H.C., M.Y., Z.X., P.X., Z.A. and H.H.; All authors have read and agreed to the published version of the manuscript.

Funding: This research was funded by the National Natural Science Foundation of China (Grant No.51974278, 52204406), the Natural Science Foundation of Hebei Province Young Fund Project (Grant No.E2020203118), the Hebei Province High Level Talent Fund Project (Grant No.B2020003013), and Qinhuangdao Science and Technology Support Plan Project (Grant No.202101A341). And CITIC Dicastal Co., thanks for their great help and suggestions in the experiment.

Data Availability Statement: No similar data were available elsewhere in the first publication.

Acknowledgments: The authors would like to thank CITIC Dicastal Co., Ltd. for the support of facilities and personnel.

Conflicts of Interest: The authors declare no conflict of interest. The sponsor had no role in the design, execution, interpretation or writing of the study. The sponsor reviewed the manuscript to ensure confidential information was not released.

Nomenclatures:

$\boldsymbol{u}$	The velocity vector of flow field, m/s
$\boldsymbol{\Psi}$	Flux of flow field
$\boldsymbol{S}$	The source term of the mass conservation equation
Γ	Diffusion coefficients of the k-ε equations, m^2/s
λ	Thermal conductivity, W/(m·°C)
ρ	Density, kg/m^3
C_P	Specific heat capacity, J/(kg·°C)
T	Transient temperature of the object, °C
t	Time, s
q	Heat flux density, W/m^2
∇T	Normal temperature gradient of the boundary layer
T_s	Surface temperature of the boundary layer, °C
T_{ref}	Temperature of the flowing fluid, °C
h	Heat exchange coefficient, $W/(m^2 \cdot °C)$

References

1. Liang, Z.L.; Li, W.T.; Zhu, B.G.; Niu, L.Q. Modelling Dynamic Recrystallization of A356 Aluminum Alloy during Hot Deformation. *Metals* **2022**, *12*, 1407. [CrossRef]
2. Li, P.; Maijer, D.M.; Lindley, T.C.; Lee, P.D. Simulating the Residual Stress in an A356 Automotive Wheel and Its Impact on Fatigue Life. *Metall. Mater. Trans. B* **2007**, *38*, 505–515. [CrossRef]
3. Hu, P.; Yang, H.; Tan, H.; Yang, L.; Sun, X. Optimization of Low Pressure Die Casting Process for Alloy Wheels with Complex Wheel Faces. *Spec. Cast. Nonferrous Alloys* **2018**, *38*, 402–405.

4. Gholamreza, K.; Mohammad, J.K.; Ali, N. Microstructure and hot deformation behavior of AlMg6 alloy produced by equal-channel angular pressing. *Mater. Sci. Eng. A* **2012**, *542*, 15–20.
5. Estey, C.M.; Cockcroft, S.L.; Maijer, D.M.; Hermesmann, C. Constitutive behaviour of A356 during the quenching operation. *Mater. Sci. Eng. A* **2004**, *383*, 245–251. [CrossRef]
6. Zhao, Y.T.; Lu, S.P.; Chen, G. *Manufacturing Technology of Light-Alloy Wheels*; China Machine Press: Beijing, China, 2018; p. 108.
7. Deng, Y.L.; Zhang, X.M. Development of aluminium and aluminium alloy. *Chin. J. Nonferrous Met.* **2019**, *29*, 2115–2141.
8. Huo, Y.C.; Liu, Y.; Huang, L.N.; Li, Q. Quenching stress at inner surface of hollow cylinders. *Trans. Mater. Heat Treat.* **2022**, *43*, 157–166.
9. Wang, W.; Zhou, J.X.; Yin, Y.J.; Shen, X.; Ji, X.Y. Simulation of Thermal Stress and Distortion during Heat treatment process of Swing at Fixed End. In Proceedings of the 2017 China Foundry Activity Week Proceedings, Soochow, China, 14 November 2017; pp. 498–504.
10. Li, H.W.; Gao, Y.F.; Du, C.H.; Hong, W.P. Numerical study on swirl cooling flow, heat transfer and stress characteristics based on fluid-structure coupling method under different swirl chamber heights and Reynolds numbers. *Int. J. Heat Mass Transf.* **2021**, *173*, 121228. [CrossRef]
11. Yan, M.; Fan, Y.R.; Yue, M.; Wei, J.N.; Lin, H.F.; Li, S.G. Heat-mass transfer coupling effects in water-ice phase transformation of water-bearing coal frozen with liquid nitrogen. *Appl. Therm. Eng.* **2022**, *215*, 118902. [CrossRef]
12. Peng, C.T.; Luo, Y.; Jin, Y. Thermal Fluid-Solid Coupling and Thermal Stress Analysis of Vacuum Valve Based on CFD. In *Proceedings of the Seventh Asia International Symposium on Mechatronics*; Springer: Singapore, 2 September 2020; pp. 85–94.
13. Ying, L.; Gao, T.H.; Dai, M.H.; Hu, P.; Teng, H. Experimental and numerical investigation on temperature field and tailored mechanical properties distribution of 22MnB5 steel in spray quenching process. *J. Manuf. Process.* **2020**, *57*, 930–956. [CrossRef]
14. Hu, H.; Yang, L.Z.; Guo, Y.F.; Chen, F.; Wang, S.; Zheng, F.Q.; Li, B. Numerical Simulation of Bottom-Blowing Stirring in Different Smelting Stages of Electric Arc Furnace Steelmaking. *Metals* **2021**, *11*, 799. [CrossRef]
15. Song, J.S.; Zhang, W.L.; Li, X.J.; Chen, R.Z.; Luo, P. Numerical simulation of dynamic quenching process of forged aluminum alloy wheel hub. *Heat Treat. Met.* **2019**, *44*, 213–217.
16. Meng, T.; Zhang, J.Y.; Li, T. Numerical Simulation and Optimization for the Temperature Field of the Coach in the Sleeping EMU. *J. Mech. Eng.* **2018**, *54*, 17–22. [CrossRef]
17. Liu, Z.W.; Yi, J.; Li, S.K.; Nie, W.J.; Li, L.X.; Wang, G. Study on inhomogeneous cooling behavior of extruded profile with unequal and large thicknesses during quenching using thermo-mechanical coupling model. *Trans. Nonferrous Met. Soc. China* **2020**, *30*, 1211–1226. [CrossRef]
18. Wang, C.T.; Li, Z.C. Numerical Simulation Research of Sequential Fluid-solid Coupling Heat Transfer of Exhaust Turbine. *J. Mech. Eng.* **2017**, *53*, 156–164. [CrossRef]
19. Roy, M.J.; Maijer, D.M.; Dancoine, L. Constitutive behavior of as-cast A356. *Mater. Sci. Eng. A* **2012**, *548*, 195–205. [CrossRef]
20. Popiel, C.O.; Wojtkowiak, J. Simple Formulas for Thermophysical Properties of Liquid Water for Heat Transfer Calculations (from 0 °C to 150 °C). *Heat Transf. Eng.* **1998**, *19*, 87–101. [CrossRef]
21. Kang, L.; Zhao, G.; Tian, N.; Zhang, H.T. Computation of synthetic surface heat transfer coefficient of 7B50 ultra-high-strength aluminum alloy during spray quenching. *Trans. Nonferrous Met. Soc. China* **2018**, *28*, 989–997. [CrossRef]
22. Pouraliakbar, H.; Firooz, S.; Jandaghi, M.R.; Khalaj, G.; Ali, N. Predicting the ultimate grain size of aluminum sheets undergone constrained groove pressing. *Int. J. Adv. Manuf. Technol.* **2016**, *86*, 1639–1658. [CrossRef]

Disclaimer/Publisher's Note: The statements, opinions and data contained in all publications are solely those of the individual author(s) and contributor(s) and not of MDPI and/or the editor(s). MDPI and/or the editor(s) disclaim responsibility for any injury to people or property resulting from any ideas, methods, instructions or products referred to in the content.